

Universality of Top Rank Statistics for Brownian Reshuffling

Zdzislaw Burda*

*AGH University of Krakow, Faculty of Physics and Applied Computer Science,
al. Mickiewicza 30, 30-059 Kraków, Poland*

Mario Kieburg†

*University of Melbourne, School of Mathematics and Statistics,
813 Swanston Street, Parkville, Melbourne VIC 3010, Australia;
Institut Mittag-Leffler, Djursholm, SE-182 60, Sweden*

We study the dynamical aspects of the top rank statistics of particles, performing Brownian motions on a half-line, which are ranked by their distance from the origin. For this purpose, we introduce an observable that we call the overlap ratio $\Omega(t)$, whose average is the probability that a particle that is on the top- n list at some time will also be on the top- n list after time t . The overlap ratio is a local observable which is concentrated at the top of the ranking and does not require the full ranking of all particles. It is simple to measure in practice. We derive an analytical formula for the average overlap ratio for a system of N particles in the stationary state that undergo independent Brownian motion on the positive real half-axis with a reflecting wall at the origin and a drift towards the wall. In particular, we show that for $N \rightarrow \infty$, the overlap ratio takes a rather simple form $\langle \Omega(t) \rangle = \text{erfc}(a\sqrt{t})$ for $n \gg 1$ with some scaling parameter $a > 0$. This result is a very good approximation even for moderate sizes of the top- n list such as $n = 10$. Moreover, as we show, the overlap ratio exhibits universal behavior observed in many dynamical systems including geometric Brownian motion, Brownian motion with a position-dependent drift and a soft barrier on one side, the Bouchaud-Mézard wealth distribution model, and Kesten processes.

I. INTRODUCTION

Rankings are important tools for data analysis; see [1]. Almost everything can be ranked, and often is: the richest people, the largest companies, the largest cities, the best universities, the income, the revenue, etc. The rankings are usually concentrated on the extreme values of a data set such as top or bottom, for instance, those who are leaders. An important and natural question is how such a ranking is going to evolve when the data set underlies some stochastic process. Such dynamical aspects of ranking statistics have recently attracted attention [2–7].

Rankings appear very naturally in physics and other disciplines. When considering a gas of distinguishable particles, for instance, one can ask which of these particles is the closest or the furthest away from a specific point and how that evolves in time. Certainly, when particles on a line strongly repel each other, the ranking will remain always the same. However, once one goes to two and higher dimensions, this is no longer the case. Even when the particles have interactions like the Coulomb interaction, it is known that the distance of the particles furthest away from a point (say the centre of mass of all particles) behave independently, see [8], so that overtaking in the ranking is permissible. Extreme occupations in the fluid phase of zero range processes [9] and extreme heights in higher dimensional random landscapes [10] follow Gumbel statistics [11] which suggest that the collection of these extreme events behave effectively independently and open the question of their rankings how that develops in time. Another prominent set of models are systems describing quantities, say $w(t)$, with dynamics driven by the rule of proportioned growth [12], for example wealth, in terms of multiplicative stochastic processes. In such a setting, the logarithm $x(t) = \ln w(t)$ evolves according to an additive stochastic process, where the instantaneous growth rates $\Delta x(t) = x(t + \Delta t) - x(t)$ at any time t are independent of or weakly dependent on $x(t)$. In this case, the process has a stationary state in which the growth rate x obeys an exponential law and, as a consequence, the quantity $w = e^x$ follows a power law (Pareto distribution) [13, 14]. Again, the question of the dynamics of the ranking of the top n and / or the bottom m is very natural.

The whole problem of ranking of the top or bottom participants belongs to the field of extreme value statistics, which has recently found much interest in statistical physics and mathematics; see the review [15]. When it comes to the ranking dynamics, one needs to choose a metric. The most popular are Spearman ρ -distance [16] and Kendall τ -distance [17]. Most of these measures take into account the total ranking of all particles. Hence, they are numerically time consuming when the set of particles is very large, and they are mostly insensitive with respect to changes in the extreme rankings. This is the reason why we will consider in the present work the observable of the overlap ratio introduced in [3]. It is a

* zdzislaw.burda@agh.edu.pl

† m.kieburg@unimelb.edu.au

particular form of the overlap coefficient in set theory [18] (also known as Szymkiewicz–Simpson coefficient), it specifies what the ratio is of the top n that will be in the top n after a time t . A probabilistic interpretation of the average overlap is the probability that the top- n remain the top- n after such a time lapse. There are also other set-theoretical distances; see [18] and references therein, but most are more involved and less intuitive, so that we stick with the simplest choice of the overlap ratio.

There are several reasons why the overlap ratio is advantageous. Firstly, it is a local quantity and does not require a ranking of the whole list. One can therefore concentrate separately on the top (leaders) or bottom (losers) of the distribution or on the bulk (typical members). Secondly, it is easily measurable. Finally, we have found that it captures universal behavior. Showing this latter and, in our eyes, most important benefit will be the main task of the present work. The idea is that universality should show once the system is in a stationary state and is large enough. Despite the global stationarity of the state, there will be some local fluctuations in the ranking. These fluctuations, we claim, are universal.

To compute the universal benchmark, we analytically study a rather simple toy model. We consider N particles on the positive real half-axis that undergo independent Brownian motions. To find a stationary state, we introduce a reflective wall at the origin and add a negative constant drift to this wall. This interplay of barrier (wall), drift, and diffusion prevents the particles furthest away from the origin to continue rising forever, which would forbid a reshuffling that would otherwise be induced by the stochastic nature of the dynamics. We compute the overlap ratio for this stochastic process of the top- n particles at finite N and then take the limit $N \rightarrow \infty$. The results we obtain will then be compared with the overlap measured of the top n list for various other stochastic processes that we numerically simulate.

The article is built as follows. In Sect. II, we briefly review the toy model of a Brownian motion of N particles on the positive real line with a reflective wall at the origin and a drift towards this wall. This setting allows for a stationary state. Despite that being in the stationary state does not show any explicit time dependence, the ranking indeed undergoes a nontrivial evolution. We analyse this evolution with the help of the average overlap ratio introduced in Sect. III and derive analytic formulas for a finite number of particles. In Sect. IV, we perform the asymptotic analysis for an infinitely large number of particles. Therein, we derive expressions for the top- n ranking with n fixed, as well as in the limit $n \rightarrow \infty$. These results are compared with the discrete-time Brownian motion in Sect. V. To highlight the universality of the results, we also compare them with the ranking statistics of other stochastic processes such as the Brownian motion with a position-dependent drift and a lower soft barrier, the geometric (multiplicative) Brownian motion, the Bouchaud–Mézard wealth distribution model [19], and Kesten processes [20], see Sect. VI. In Sect. VII, we summarise our findings and point out open problems that have arisen from our investigations. Some analytical considerations for the Brownian motion on the positive real line, the overlap ratio and details of some asymptotic analysis calculation can be found in the Appendices A, B and C, respectively.

II. DIFFUSION MODEL

The stochastic model, of which we are convinced it produces a universal dynamical rank statistic, is a gas of N independent particles performing independent Brownian motion on \mathbb{R}_+ in the presence of a reflective hard wall at the origin $x = 0$ and a drift μ towards the wall. The positions of these particles at time t will be denoted by $x_j(t)$, $j = 1, \dots, N$. Diffusion of such a system, with a diffusion constant $\sigma^2/2$, is described by a Fokker–Planck equation for the probability density $p(x, t)$ for finding particles at the position $x \geq 0$ at time $t \geq 0$,

$$\partial_t p(x, t) = -\mu \partial_x p(x, t) + \frac{\sigma^2}{2} \partial_x^2 p(x, t). \quad (1)$$

The reflection at the wall at $x = 0$ is enforced by the boundary condition

$$-\mu p(0, t) + \frac{\sigma^2}{2} \partial_x p(0, t) = 0, \quad (2)$$

which means that there is no probability current passing through the wall. The initial probability density at time $t = 0$ is given in shorthand by

$$p(x, 0) = p_0(x) \quad \text{for } x \geq 0. \quad (3)$$

Since all particles forming the gas are subject to the same dynamics, the equations are independent of the particle index j .

A. The one particle solution

The differential equation (1) with boundary condition (2) and initial condition (3) has been solved in [22, 23]. It exhibits the following behaviour. If $\mu > 0$, the particles flow away from the origin. Thence, for large time $t > 0$ the initial

condition is washed out and the hard wall becomes obsolete. The whole process becomes an ordinary Brownian motion with a drift, i.e.,

$$p_{\mu>0}(x, t \gg 1) \approx \frac{1}{\sqrt{2\pi\sigma^2 t}} \exp\left[-\frac{1}{2\sigma^2 t}(x - \mu t)^2\right]. \quad (4)$$

Also for $\mu = 0$, the diffusion wins against the initial condition, though the reflective wall is now visible so that

$$p_{\mu=0}(x, t \gg 1) \approx 2\sqrt{\frac{1}{2\pi\sigma^2 t}} \exp\left[-\frac{x^2}{2\sigma^2 t}\right]. \quad (5)$$

The additional factor of 2 compared to (5) is due to condition $x > 0$, which was irrelevant in the case of $\mu > 0$. The only situation where a stationary solution exists is for $\mu < 0$. Then, the drift to the hard wall and the diffusion reach a balance and create the unique profile

$$p_{\mu<0}(x, t \gg 1) \approx p_{\text{stat}}(x) = \frac{2|\mu|}{\sigma^2} \exp\left[-\frac{2|\mu|}{\sigma^2} x\right]. \quad (6)$$

This latter case is the situation we are interested in and where non-trivial rank statistics are attained.

Considering (6), it is convenient to introduce the parameter $\alpha = -2\mu/\sigma^2$ which captures the relative strength of the diffusion constant and the drift. In fact, the differential equation (1) and its boundary condition (2) are scale invariant under $(\mu, \sigma^2, 1/t) \rightarrow \lambda(\mu, \sigma^2, 1/t)$ for any $\lambda > 0$. Thus, it is useful to go over to a rescaled time $\tau = \sigma^2 t$. This especially shows that everything is captured when setting $\sigma^2 = 1$ in (1) and (2) and then rescale $t \rightarrow \sigma^2 t$. In these new units, the above equations take the form

$$\partial_t p(x, t) = \frac{\alpha}{2} \partial_x p(x, t) + \frac{1}{2} \partial_x^2 p(x, t). \quad (7)$$

and

$$\alpha p(0, t) + \partial_x p(0, t) = 0 \quad \text{for } t > 0 \quad \text{and} \quad p(x, 0) = p_0(x) \quad \text{for } x \geq 0. \quad (8)$$

The solution of (7) with these boundary and initial conditions can be written in terms of the heat kernel (Green's function)

$$p(x, t) = \int_0^\infty p(y, 0) K(y, x, t) dy, \quad (9)$$

which has the form [22, 23]

$$K(y, x, t) = \partial_x F(y, x, t) \quad (10)$$

where

$$F(y, x, t) = \frac{1}{2} \operatorname{erfc}\left[\frac{2(y-x) - \alpha t}{\sqrt{8t}}\right] - \frac{1}{2} e^{-\alpha x} \operatorname{erfc}\left[\frac{2(y+x) - \alpha t}{\sqrt{8t}}\right]. \quad (11)$$

for any $x, y \geq 0$ and $t > 0$. The function $F(y, x, t)$ is the probability that a particle that initially was in position y , will be in the interval $[0, x]$ at time t , so it is just the cumulative density function for the probability distribution at time t conditioned on initial position y ,

$$F(y, x, t) = \int_0^x K(y, x', t) dx'. \quad (12)$$

Certainly, it is $F(y, 0, t) = 0$ and $F(y, \infty, t) = 1$.

The first term in $F(y, x, t)$ corresponds to the diffusion towards the wall, while the second corresponds to the diffusion away from the wall. The initial position y is seen as mirrored: $-y$ in the second term. The relative contribution of the two terms is $e^{\alpha x}$ as it comes from the drift factors $e^{\pm\alpha/2x}$ toward and away from the wall.

It is straightforward to check that the kernel satisfies the following equations

$$\partial_t K(y, x, t) = \frac{\alpha}{2} \partial_x K(y, x, t) + \frac{1}{2} \partial_x^2 K(y, x, t) \quad (13)$$

with

$$\alpha K(y, 0, t) + \partial_x K(y, 0, t) = 0 \quad \text{and} \quad K(y, x, 0) = \lim_{t \rightarrow 0} K(y, x, t) = \delta(x - y), \quad (14)$$

for all $y, x \geq 0$ and $t > 0$.

For completeness, we present the derivation of the heat kernel in Appendix A. A very important feature of the kernel is that it leads to a function that is independent of the initial position y in the limit $t \rightarrow \infty$, i.e., for $\alpha > 0$ it is

$$p_{\text{stat}}(x) \equiv K(y, x, \infty) \equiv \lim_{t \rightarrow \infty} K(y, x, t) = \alpha e^{-\alpha x}. \quad (15)$$

As a consequence, independently of the initial distribution $p(y, 0) = p_0(y)$, the system will end up in the state described by the probability density $p_{\text{stat}}(x)$. Clearly p_{stat} is the stationary state of the evolution operator

$$p_{\text{stat}}(x) = \int_0^\infty p_{\text{stat}}(y) K(y, x, t) dy \quad (16)$$

for any $y, x, t \geq 0$.

B. Brownian shuffle

Next, we move from the single-particle solution to the solution of N independent particles. We assume that the initial positions of the particles are at $y_1 \geq y_2 \geq \dots \geq y_N$. The particles are indexed according to their initial value, from highest to lowest. The corresponding joint probability distribution is then

$$p(y_1, \dots, y_N; x_1, \dots, x_N; t) = \prod_{j=1}^N K(y_j, x_j, t), \quad (17)$$

where x_j is the position of the particle j at time $t > 0$ that initially was at y_j . We would like to stress that, unlike the positions $y_1 \geq y_2 \geq \dots \geq y_N$, the positions x_1, \dots, x_N are not ordered. Surely, the order changes over time as the particles perform independent Brownian motions. The statistics of this change shall be investigated.

For this purpose, we consider the probability that the particle j , which initially has the j -th largest value, will have the k -th largest value at time t . This probability can be made explicit by the formula

$$\begin{aligned} P(k; j; t | y_1, \dots, y_N) &= \int_0^\infty dx K(y_j, x, t) \frac{1}{(k-1)!} \partial_z^{k-1} \prod_{l \neq j} (F(y_l, x, t) + z(1 - F(y_l, x, t))) \Big|_{z=0} \\ &= \int_0^\infty dx \oint \frac{dz}{2\pi i z^k} \partial_x F(y_j, x, t) \prod_{l \neq j} (z + (1-z)F(y_l, x, t)). \end{aligned} \quad (18)$$

In the second equality we replaced the derivative ∂_z^{k-1} with a contour integral on the complex plane over a small circle around the origin $|z| = \epsilon < 1$. As we shall see, this method sometimes makes calculations easier.

The interpretation of this formula is as follows. The $(k-1)$ -th derivative with respect to z at $z=0$ selects the $k-1$ particles whose positions are larger than x , being the position of the j -th particle at time t . The remaining $N-k$ particles, excluding the j -th particle, will then have a position smaller than x . Hence, the coefficient at the term z^{k-1} of the polynomial obtained after multiplying all the factors in the product (18) contains all combinations of products of $k-1$ probabilities $1 - F(y_l, x, t)$ for x_l greater than x and all combinations of products of $N-k$ probabilities $F(y_l, x, t)$ for x_l smaller than x .

Surely, the identities

$$\sum_{j=1}^N P(k; j; t | y_1, \dots, y_N) = 1 \quad \text{and} \quad \sum_{k=1}^N P(k; j; t | y_1, \dots, y_N) = 1 \quad (19)$$

must hold true for all initial positions $y_1 \geq y_2 \geq \dots \geq y_N$ and all times $t > 0$. The first identity reflects that the j -th particle must be at some position in the ordering, which is certainly always true, while the second identity says that one of the N particles will always be at position k , which is also a true statement. The identities (19) are proven in Appendix B.

III. OVERLAP RATIO UNDER BROWNIAN SHUFFLING

We are interested in the top- n particles, which is an ordered list of the n elements with the n largest values in the population. The overlap ratio between two top- n lists, taken from the same population at different times, is the quotient of the number of elements present in both lists and the length of the list n . In this way, this observable will remain

bounded by unity even when taking the limit $n \rightarrow \infty$, too. To have a well-posed initial condition for any n we need to assume the stronger ordering of the positions $y_1 > y_2 > \dots > y_N$.

We denote by j the j -th highest position in the ranking at time zero, and by $\sigma_t(j)$ its position in the ranking at time t . The overlap rate is, then, explicitly

$$\Omega_n(t) = \frac{1}{n} \sum_{j=1}^n \Theta(n - \sigma_t(j)), \quad (20)$$

where Θ is the Heaviside step function, meaning it vanishes for $x < 0$ and is unity otherwise. The overlap ratio is a particular form of the Szymkiewicz–Simpson coefficient [18] for the set of the top n lists at the beginning and at time t .

A. The general setting

For a gas consisting of N Brownian diffusing particles with initial positions $y_1 > y_2 > \dots > y_N$, the average overlap ratio after time t can be expressed in terms of the transition probability (18), i.e.,

$$\langle \Omega_n(t) \rangle_{y_1, \dots, y_N} = \frac{1}{n} \sum_{j,k=1}^n P(k; j; t | y_1, \dots, y_N). \quad (21)$$

We denote the ensemble average under the condition of initial positions by $\langle \cdot \rangle_{y_1, \dots, y_N}$. The double sum sums up the probabilities that any of the top- n particles still remain in the top- n . Surely, the ordering inside the top n may have changed.

Probabilistic initial conditions cover a more general setting. Since the particles do not interact with each other, we can restrict our considerations to Poisson initial conditions, where the joint probability density is the product of the single-particle probability density

$$p_0(r_1, \dots, r_N) = \prod_{j=1}^N p_0(r_j). \quad (22)$$

We note that the initial positions r_1, \dots, r_N are unordered unlike $y_1 > y_2 > \dots > y_N$. The transition probability for the probabilistic initial conditions can be found in a similar way as in the case of (18). The only difference is that we need to include the initial ordering in the integral. We implement this in the same way for the final position, namely by a derivative with respect to an auxiliary variable,

$$P(k; j; t | p_0) = N \int_0^\infty dx \int_0^\infty dr K(r, x, t) p_0(r) \times \frac{1}{(k-1)!(j-1)!} \partial_w^{k-1} \partial_z^{j-1} \left(\left[\int_0^r +z \int_r^\infty \right] \left[\int_0^x +w \int_x^\infty \right] K(r', x', t) p_0(r') dx' dr' \right)^{N-1} \Big|_{w=z=0}. \quad (23)$$

The derivatives ∂_w^{k-1} and ∂_z^{j-1} can be anew replaced by contour integrals in the complex plane over circles with the center at the origin and a suitably small radius $\epsilon \ll 1$. The expression in the parentheses can be rewritten as $wP_z(r) + (1-w)G_z(r, x, t)$ with

$$P_z(r) = P_-(r) + zP_+(r) \quad \text{and} \quad G_z(r, x, t) = G_-(r, x, t) + zG_+(r, x, t), \quad (24)$$

where it is $P_-(r) = \int_0^r p_0(r') dr'$, $P_+(r) = 1 - P_-(r)$, and

$$G_-(r, x, t) = \int_0^r F(r', x, t) p_0(r') dr' \quad \text{and} \quad G_+(r, x, t) = \int_r^\infty F(r', x, t) p_0(r') dr'. \quad (25)$$

With the help of this notation we obtain

$$P(k; j; t | p_0) = N \int_0^\infty dx \int_0^\infty dr K(r, x, t) p_0(r) \oint \frac{dz}{2\pi i z^j} \oint \frac{dw}{2\pi i w^k} (wP_z(r) + (1-w)G_z(r, x, t))^{N-1}. \quad (26)$$

To find this result one needs to apply $\int_0^x K(r', x', t) dx' = 1 - \int_x^\infty K(r', x', t) dx'$,

$$\left[\int_0^x +w \int_x^\infty \right] K(r', x', t) dx' = (1-w)F(r', x, t) + w, \quad (27)$$

cf., Eq. (12).

Similarly to equation (19), it is straightforward to check that the sum rules

$$\sum_{j=1}^N P(k; j; t|p_0) = 1 \quad \text{and} \quad \sum_{k=1}^N P(k; j; t|p_0) = 1 \quad (28)$$

are satisfied, see Appendix B.

The overlap ratio for the initial condition p_0 can be calculated by summing over $j, k = 1, \dots, n$ in (26), analogously to (21). These sums are two independent geometric sums; for instance, for $1/z^j$ it leads to $(1 - z^{-n})/(z - 1) = 1/(z - 1) - 1/[(1 - z)z^n]$. The integral of the first term $1/(z - 1)$ vanishes as the origin is no longer a pole, so we only have $-1/[(1 - z)z^n]$. A similar summation rule can be applied to the sum over w . Hence, we arrive at the expression

$$\langle \Omega_n(t) \rangle_{p_0} = \frac{N}{n} \int_0^\infty dx \int_0^\infty dr K(r, x, t) p_0(r) \oint \frac{dz}{2\pi i (1 - z) z^n} \oint \frac{dw}{2\pi i (1 - w) w^n} (w P_z(r) + (1 - w) G_z(r, x, t))^{N-1}. \quad (29)$$

To keep the notation simple, we denote the ensemble average under the initial condition $p(x, 0) = p_0(x)$ by $\langle \cdot \rangle_{p_0}$.

B. Overlap ratio for stationary state

For large t and for a drift to the hard wall, we know that the gas of particles equilibrates at the stationary state following the distribution (15). Thus, it is natural to assume that the overlap ratio statistics will follow (29) with $p_0(r) = p_{\text{stat}}(r)$ when $t \rightarrow \infty$. Hence, we aim to calculate the overlap ratio for the stationary state.

As follows from (16) the single particle distribution $p(r, t)$ at any moment of time is identical to that at the beginning $p(r, t) = p_0(r) = p_{\text{stat}}(r)$. As a consequence, also the joint probability distribution is constant in time.

$$p(r_1, \dots, r_N; t) = p_0(r_1, \dots, r_N) = \prod_{j=1}^N p_{\text{stat}}(r_j) \quad (30)$$

Statistically speaking, the total system looks identical at every moment. However, the positions of the particles will shuffle over time, so that the overlap will not be constant as we shall see.

The average overlap, which we denote as $\langle \Omega_n(t) \rangle_{N, \alpha}$ for the stationary state, depends on the size of the top- n list size, the total size of the system N , the stationary state parameter α , see (15), and the time elapsed between the recordings of the top- n lists. Using (29) we find

$$\langle \Omega_n(t) \rangle_{N, \alpha} = \frac{1}{n!(n-1)!} \partial_z^{n-1} \partial_w^{n-1} Z_N^{(\alpha)}(z, w, t) \Big|_{z=w=0} \quad (31)$$

where

$$\begin{aligned} Z_N^{(\alpha)}(z, w, t) &= \frac{N}{(1-z)(1-w)} \int_0^\infty dx \int_0^\infty dr K(r, x, t) \alpha e^{-\alpha r} \\ &\times [w(1 + (z-1)e^{-\alpha r}) + (1-w)(G_-(r, x, t) + zG_+(r, x, t))]^{N-1}. \end{aligned} \quad (32)$$

We already plugged in

$$P_z(r) = \left[\int_0^r + z \int_r^\infty \right] dr' \alpha e^{-\alpha r'} = 1 + (z-1)e^{-\alpha r}. \quad (33)$$

The functions $G_\pm(r, x, t)$ are incomplete Gaussian integrals once we plug the stationary state $p_0(r) = p_{\text{stat}}(r)$ and (11) into (25), which yields complementary error functions

$$\begin{aligned} G_-(r, x, t) &= \frac{1}{2} \left(2 - \operatorname{erfc} \left[\frac{2r + 2x + \alpha t}{\sqrt{8t}} \right] - e^{-\alpha x} \left(2 - \operatorname{erfc} \left[\frac{2r - 2x + \alpha t}{\sqrt{8t}} \right] \right) \right. \\ &\quad \left. - e^{-\alpha r} \left(2 - \operatorname{erfc} \left[\frac{2x - 2r + \alpha t}{\sqrt{8t}} \right] \right) + e^{-\alpha(r+x)} \operatorname{erfc} \left[\frac{2r + 2x - \alpha t}{\sqrt{8t}} \right] \right), \\ G_+(r, x, t) &= \frac{1}{2} \left(\operatorname{erfc} \left[\frac{2r + 2x + \alpha t}{\sqrt{8t}} \right] - e^{-\alpha x} \operatorname{erfc} \left[\frac{2r - 2x + \alpha t}{\sqrt{8t}} \right] \right. \\ &\quad \left. + e^{-\alpha r} \left(2 - \operatorname{erfc} \left[\frac{2x - 2r + \alpha t}{\sqrt{8t}} \right] \right) - e^{-\alpha(r+x)} \operatorname{erfc} \left[\frac{2r + 2x - \alpha t}{\sqrt{8t}} \right] \right). \end{aligned} \quad (34)$$

Equation (31) shows that the overlap ratios are essentially the Taylor series coefficients of $Z_N^{(\alpha)}(z, w, t)$ in variables z and w about the point $w = z = 0$ at powers $(zw)^{n-1}$. For instance in the simplest case of $n = 1$, the overlap ratio takes the simple form

$$\langle \Omega_1(t) \rangle_{N,\alpha} = \alpha N \int_0^\infty dx \int_0^\infty dr K(r, x, t) e^{-\alpha r} G_-^{N-1}(r, x, t). \quad (35)$$

The overlap ratio $\langle \Omega_1(t) \rangle_{N,\alpha}$ is simply the probability that the current leader will be the leader at time t . In a similar way, we derive explicit integral expressions for $\langle \Omega_2(t) \rangle_{N,\alpha}$, $\langle \Omega_3(t) \rangle_{N,\alpha}$, *etc.* from $Z_N^{(\alpha)}(z, w, t)$. The integral expressions can be used to numerically compute the overlap ratios.

IV. ASYMPTOTIC ANALYSIS FOR $N \rightarrow \infty$

We would expect that the behaviour of the overlap ratios computed from the stationary state is universal only when the system size becomes infinitely large, i.e., $N \rightarrow \infty$. Indeed, under rather general conditions, especially that no Lévy flights are present, a system with many participants will behave like a Brownian motion. Thence, our next goal is to analyse the asymptotic of (32) for $N \rightarrow \infty$ and $n \ll N$.

A. Analysis for short top lists

As we consider independent particles drawn from the stationary state $p_{\text{stat}}(r) = \alpha e^{-\alpha r}$, the largest particles will follow Gumble statistics, in particular the distribution of the position of the j -th top particle will be

$$\tilde{p}_{\text{top},j}(r) = \frac{\alpha N!}{(N-j)!(j-1)!} e^{-j\alpha r} (1 - e^{-\alpha r})^{N-j} \approx \frac{\alpha}{(j-1)!} e^{-j(\alpha r - \ln N)} \exp[-e^{-(\alpha r - \ln N)}]. \quad (36)$$

Therefore, the highest values are located near $\ln N/\alpha$. The dominant contribution to the integral (32) for $N \rightarrow \infty$, can, then, be obtained by going over to the new variables ξ and ζ ,

$$r = \frac{\ln N}{\alpha} + \zeta, \quad x = \frac{\ln N}{\alpha} + \xi. \quad (37)$$

The functions appearing in the integral (32) can be expanded in $1/N$

$$\begin{aligned} K\left(\frac{\ln N}{\alpha} + \zeta, \frac{\ln N}{\alpha} + \xi, t\right) &= k(\zeta, \xi, t) + O(1/N), \\ G_- \left(\frac{\ln N}{\alpha} + \zeta, \frac{\ln N}{\alpha} + \xi, t\right) &= 1 - \frac{1}{N} g_-(\zeta, \xi, t) + O(1/N^2), \\ G_+ \left(\frac{\ln N}{\alpha} + \zeta, \frac{\ln N}{\alpha} + \xi, t\right) &= -\frac{1}{N} g_+(\zeta, \xi, t) + O(1/N^2), \end{aligned} \quad (38)$$

where

$$\begin{aligned} k(\zeta, \xi, t) &= \sqrt{\frac{1}{2\pi t}} \exp\left[-\frac{[2(\zeta - \xi) - \alpha t]^2}{8t}\right], \\ g_-(\zeta, \xi, t) &= \frac{1}{2} \left[e^{-\alpha \xi} \left(2 - \operatorname{erfc}\left[\frac{2\zeta - 2\xi + \alpha t}{\sqrt{8t}}\right] \right) + e^{-\alpha \zeta} \left(2 - \operatorname{erfc}\left[\frac{2\xi - 2\zeta + \alpha t}{\sqrt{8t}}\right] \right) \right], \\ g_+(\zeta, \xi, t) &= \frac{1}{2} \left[e^{-\alpha \xi} \operatorname{erfc}\left[\frac{2\zeta - 2\xi + \alpha t}{\sqrt{8t}}\right] - e^{-\alpha \zeta} \left(2 - \operatorname{erfc}\left[\frac{2\xi - 2\zeta + \alpha t}{\sqrt{8t}}\right] \right) \right]. \end{aligned} \quad (39)$$

Moreover, we exploit $e^{-\alpha r} = e^{-\alpha \zeta}/N$ and $g_+(\zeta, \xi, t) = e^{-\alpha \zeta} - g_-(\zeta, \xi, t)$ to recast (32) into

$$\begin{aligned} Z_N^{(\alpha)}(z, w, t) &= \frac{\alpha}{(1-z)(1-w)} \int_{-\ln N/\alpha}^\infty d\xi \int_{-\ln N/\alpha}^\infty d\zeta (k(\zeta, \xi, t) e^{-\alpha \zeta} + O(1/N)) \\ &\quad \times \left[1 - \frac{1}{N} \left(w(1-z) e^{-\alpha \zeta} + z(1-w) e^{-\alpha \xi} + (1-z)(1-w) g_-(\zeta, \xi, t) \right) + O(1/N^2) \right]^{N-1}. \end{aligned} \quad (40)$$

Taking the limit $N \rightarrow \infty$ gives

$$Z^{(\alpha)}(z, w, t) = \frac{\alpha}{(1-z)(1-w)} \int_{-\infty}^{\infty} d\xi \int_{-\infty}^{\infty} d\zeta k(\zeta, \xi, t) e^{-\alpha\zeta} \times \exp[-w(1-z)e^{-\alpha\zeta} - z(1-w)e^{-\alpha\xi} - (1-z)(1-w)g_-(\zeta, \xi, t)]. \quad (41)$$

Changing the integration variables to $R = (\xi + \zeta)/2$ and $s = (\xi - \zeta)/\sqrt{2t}$ and performing the integral with respect to R , we finally obtain

$$\bar{Z}^{(\alpha)}(z, w, t) = Z_*(z, w, t_*) \quad (42)$$

where

$$t_* = \frac{\alpha^2 t}{8} \quad (43)$$

and

$$Z_*(z, w, t_*) = \frac{e^{-t_*}}{\sqrt{\pi}} \frac{1}{(1-z)^2(1-w)^2} \int_{-\infty}^{\infty} ds \frac{e^{-s^2}}{e^{-2s\sqrt{t_*}} \left(\frac{1}{1-z} - \frac{1}{2} \operatorname{erfc}[\sqrt{t_*} - s] \right) + e^{2s\sqrt{t_*}} \left(\frac{1}{1-w} - \frac{1}{2} \operatorname{erfc}[\sqrt{t_*} + s] \right)}. \quad (44)$$

We see that the result depends on α only through the rescaled time variable t_* . Expanding $Z_*(z, w, t_*)$ in z and w , we find overlaps as coefficients at the powers $(zw)^{n-1}$. In particular, for $n = 1$ it is

$$\langle \Omega_1(t) \rangle_\alpha \stackrel{N \gg 1}{\approx} \Omega_{*1}(t_*) = \frac{e^{-t_*}}{\sqrt{\pi}} \int_{-\infty}^{\infty} ds \frac{e^{-s^2}}{e^{-2s\sqrt{t_*}} \left(1 - \frac{1}{2} \operatorname{erfc}[\sqrt{t_*} - s] \right) + e^{2s\sqrt{t_*}} \left(1 - \frac{1}{2} \operatorname{erfc}[\sqrt{t_*} + s] \right)}, \quad (45)$$

and for $n = 2$ we find

$$\langle \Omega_2(t) \rangle_\alpha \stackrel{N \gg 1}{\approx} \Omega_{*2}(t_*) = \frac{e^{-t_*}}{\sqrt{\pi}} \int_{-\infty}^{\infty} ds e^{-s^2} \left(\frac{1}{q^3(s, t_*)} - \frac{e^{2s\sqrt{t_*}} + e^{-2s\sqrt{t_*}}}{q^2(s, t_*)} + \frac{2}{q(s, t_*)} \right) \quad (46)$$

where

$$q(s, t_*) = e^{-2s\sqrt{t_*}} \left(1 - \frac{1}{2} \operatorname{erfc}[\sqrt{t_*} - s] \right) + e^{2s\sqrt{t_*}} \left(1 - \frac{1}{2} \operatorname{erfc}[\sqrt{t_*} + s] \right) \quad (47)$$

is the denominator in the fraction in (45).

In principle, we can find an explicit formula for any n in the form of an integral over one variable, as we illustrate below. Using (42) as a starting point, we have the relation

$$\langle \Omega_n(t) \rangle_\alpha \stackrel{N \gg 1}{\approx} \Omega_{*n}(t_*) = \frac{1}{n} \oint \frac{dz}{2\pi i z^n} \oint \frac{dw}{2\pi i w^n} Z_*(z, w, t_*) \quad (48)$$

where the contours are circles centered at $z = 0$ and $w = 0$ with a suitably small radius $\epsilon \ll 1$. Changing integration variables $u = 1/(1-z) - 1$ and $v = 1/(1-w) - 1$ in (48) with $Z_*(z, w, t_*)$ given by (44), we obtain

$$\Omega_{*n}(t_*) = \frac{e^{-t_*}}{n\sqrt{\pi}} \int_{-\infty}^{\infty} ds e^{-s^2} \oint \frac{dv}{2\pi i} \oint \frac{du}{2\pi i} \frac{(1+1/v)^n (1+1/u)^n}{e^{-2s\sqrt{t_*}u} + e^{2s\sqrt{t_*}v} + q(s, t_*)}. \quad (49)$$

Applying the binomial expansion formula for the powers in the numerator and the geometric series expansion for the expression in the denominator, and choosing terms of order $1/u$ and $1/v$, we get

$$\Omega_{*n}(t_*) = \frac{e^{-t_*}}{n\sqrt{\pi}} \int_{-\infty}^{\infty} ds e^{-s^2} \sum_{j,k=1}^n (-1)^{j+k} \binom{n}{j} \binom{n}{k} \binom{j+k-2}{j-1} e^{2(k-j)s\sqrt{t_*}} \left(\frac{1}{q(s, t_*)} \right)^{j+k-1}. \quad (50)$$

For $n = 2$ this gives $\Omega_{*2}(t_*)$, cf., (46). In general, one can find an explicit form of the integrand for any n and then perform the integration numerically. It becomes tedious as n increases but is doable. Therefore, we strive for an approximation when $n \gg 1$, which is given in the next section.

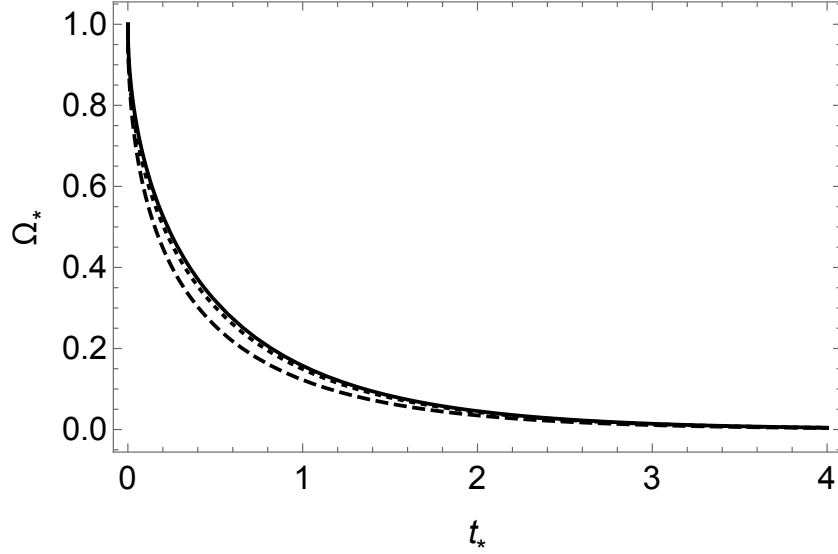


FIG. 1. The overlap ratio vs. rescaled time for $n = 1, 5, \infty$ (dashed, dotted, solid) obtained using Eqs. (50) and (57), respectively. The rescaled time t_* is given by (43). If we were to draw the corresponding curve for $n = 10$, using the line width as in the plot, it would coincide with the curve for $n = \infty$.

B. Asymptotic result for long top lists

We employ an integral representation of the third binomial in (50)

$$\binom{j+k-2}{j-1} = \oint \frac{dz}{2\pi iz} \frac{(1+z)^{j+k-2}}{z^{j-1}} = \oint \frac{dz}{2\pi iz} (1+z^{-1})^{j-1} (1+z)^{k-1}, \quad (51)$$

where the integral is over a small circle centred at $z = 0$ with a suitably small radius $\epsilon < 1$. Then, the binomial sums over j and k factorise,

$$\Omega_{*n}(t_*) = \frac{e^{-t_*}}{n\sqrt{\pi}} \int_{-\infty}^{\infty} ds e^{-s^2} \oint \frac{dz}{2\pi iz} \frac{q(s, t_*)}{(1+z^{-1})(1+z)} \sum_{j=1}^n \binom{n}{j} \left(-(1+z^{-1}) \frac{e^{-2s\sqrt{t_*}}}{q(s, t_*)} \right)^j \sum_{k=1}^n \binom{n}{k} \left(-(1+z) \frac{e^{2s\sqrt{t_*}}}{q(s, t_*)} \right)^k. \quad (52)$$

The sum over j can be extended by including the term for $j = 0$ for which the contour integral gives zero, so we get

$$\Omega_{*n}(t_*) = \frac{e^{-t_*}}{n\sqrt{\pi}} \int_{-\infty}^{\infty} ds e^{-s^2} \oint \frac{dz}{2\pi iz} \frac{q(s, t_*)}{(1+z^{-1})(1+z)} \left(1 - (1+z^{-1}) \frac{e^{-2s\sqrt{t_*}}}{q(s, t_*)} \right)^n \left[\left(1 - (1+z) \frac{e^{2s\sqrt{t_*}}}{q(s, t_*)} \right)^n - 1 \right]. \quad (53)$$

We show in Appendix (C) that for $n \rightarrow \infty$ the integral approaches the limit $\Omega_{*n}(t_*) \rightarrow \Omega_*(t_*)$, which takes the form

$$\Omega_*(t_*) = \frac{e^{-t_*}}{\sqrt{\pi}} \int_{-\infty}^{\infty} ds e^{-s^2} \int_{-\infty}^{\infty} \frac{dy}{2\pi} \frac{q(s, t_*)}{(1+iy)^2} \exp \left[(1+iy) \frac{e^{-2s\sqrt{t_*}}}{q(s, t_*)} \right] \left(1 - \exp \left[-(1+iy) \frac{e^{2s\sqrt{t_*}}}{q(s, t_*)} \right] \right). \quad (54)$$

We can simplify this expression by changing the integration variable $\tilde{y} = (1+iy)/q(s, t_*)$

$$\Omega_*(t_*) = \frac{e^{-t_*}}{\sqrt{\pi}} \int_{-\infty}^{\infty} ds e^{-s^2} \int_{\gamma} \frac{d\tilde{y}}{2\pi i \tilde{y}^2} \exp \left[\tilde{y} e^{-2s\sqrt{t_*}} \right] \left(1 - \exp \left[-\tilde{y} e^{2s\sqrt{t_*}} \right] \right). \quad (55)$$

where γ is a vertical line $\text{Re } \gamma = 1/q(s, t_*)$ extending from $-\infty$ to $+\infty$. We notice that the dependency on $q(s, t_*)$ has essentially disappeared as we are allowed to shift the contour parallel to the positive real axis without changing the result due to Cauchy's theorem (as long as no simple pole is crossed by the contour while it is being shifted).

The integral over γ can be calculated using the residue theorem. It is convenient to split it into two integrals:

$$\Omega_*(t_*) = \frac{e^{-t_*}}{\sqrt{\pi}} \int_{-\infty}^{\infty} ds e^{-s^2} \left(\int_{\gamma} \frac{d\tilde{y}}{2\pi i \tilde{y}^2} \exp \left[\tilde{y} e^{-2s\sqrt{t_*}} \right] - \int_{\gamma} \frac{d\tilde{y}}{2\pi i \tilde{y}^2} \exp \left[\tilde{y} (e^{-2s\sqrt{t_*}} - e^{2s\sqrt{t_*}}) \right] \right). \quad (56)$$

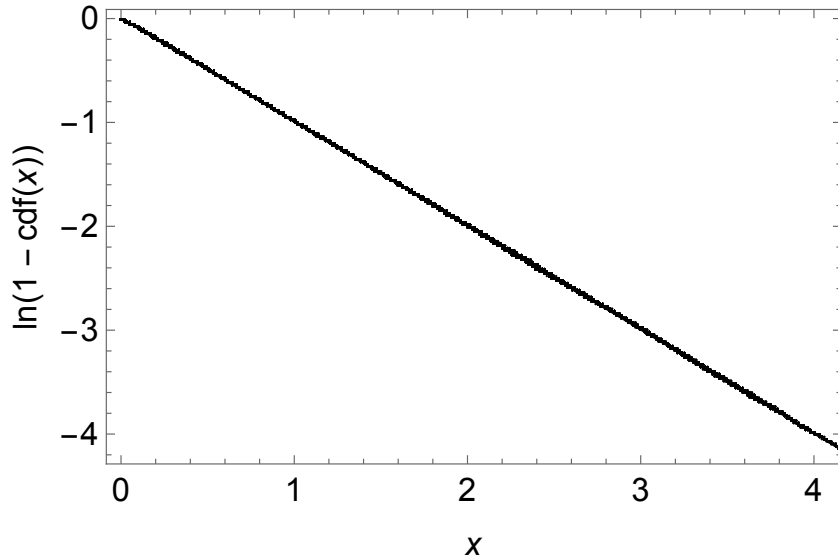


FIG. 2. The cumulative density function for the discrete time formalism is computed numerically from a population of N particles at some time k as a rank plot made of pairs of points $(x_i(k), i/N)$, for $i = 1, \dots, N$, where $x_i(k)$'s are sorted $x_1(k) \leq \dots \leq x_N(k)$. The time k is long enough to ensure that the system is in a stationary state. We plot the data for two times k and $k + 10^3$ to check that the system has indeed already reached a stationary state. On the vertical axis we plot $y = \ln(1 - P_-(x))$ which for the exponential distribution is $y = -\alpha x$. In the simulation we used $N = 10^5$, $\Delta t = 0.05$, $\alpha = 1$ and $k = 10^4$. Initially the particle positions were distributed according to the uniform distribution on $[0, 1]$. The graph shows that the system has reached a stationary state, because the data points for k and $k + 10^3$ lie almost on top of each other. They also lie on top of the curve $y = -\alpha x$ which is drawn as a thin solid line.

The first integral can be calculated by closing the contour γ to the left. In contrast, we have a case discussion for the second term, where we close the contour to the left when $s < 0$ and to the right when $s > 0$. The latter would yield zero, as there is no singularity on that side. Therefore, we obtain

$$\Omega_*(t_*) = \frac{e^{-t_*}}{\sqrt{\pi}} \int_{-\infty}^{\infty} ds e^{-s^2} \left(e^{-2s\sqrt{t_*}} - \Theta(-s) \left(e^{-2s\sqrt{t_*}} - e^{2s\sqrt{t_*}} \right) \right) = \operatorname{erfc}(\sqrt{t_*}) \quad (57)$$

with $\Theta(s)$ the Heaviside step function.

In summary, for $n \rightarrow \infty$ the mean value of the overlap ratio, $\langle \Omega_n(t) \rangle \rightarrow \langle \Omega(t) \rangle$, takes a very simple form

$$\langle \Omega(t) \rangle = \operatorname{erfc} \left(\sqrt{\frac{\alpha^2 t}{8}} \right). \quad (58)$$

In Fig. 1, we compare the overlap ratio for finite n , see Eq. (50), to the limiting result (57) for $n \rightarrow \infty$. Already, the curve for $n = 1$ lies very close to the limiting curve for $n = \infty$, while the curve for $n = 5$ touches the limiting curve almost everywhere. Thus, there is a fast convergence in n . The curves for finite n are obtained by the numerical integration of (50).

V. NUMERICAL SIMULATIONS OF DIFFUSION ON HALF-AXIS

In this section, we discuss Monte Carlo simulations of the same model but formulated in the discrete-time formalism, in which the time is indexed by an integer. We consider a gas consisting of N independent particles diffusing in one dimension, whose positions $x_j(k)$, $j = 1, 2, \dots, N$ at time k obey the following evolution equation

$$x_j(k) = |x_j(k-1) + g_j(k)| \quad (59)$$

where for all $j = 1, \dots, N$ and $k = 1, 2, \dots$ the variables $g_j(k)$ are independently identically normal distributed random numbers with mean $\mu \Delta t$ and variance $\sigma^2 \Delta t$. If there was no absolute value on the right-hand side, the equation would describe random walk (diffusion) on the real axis. The absolute value acts like a reflecting wall that changes the sign of $x_j(k-1) + g_j(k)$ every time it becomes negative, and thus keeps the particles on the positive half-axis. The continuum

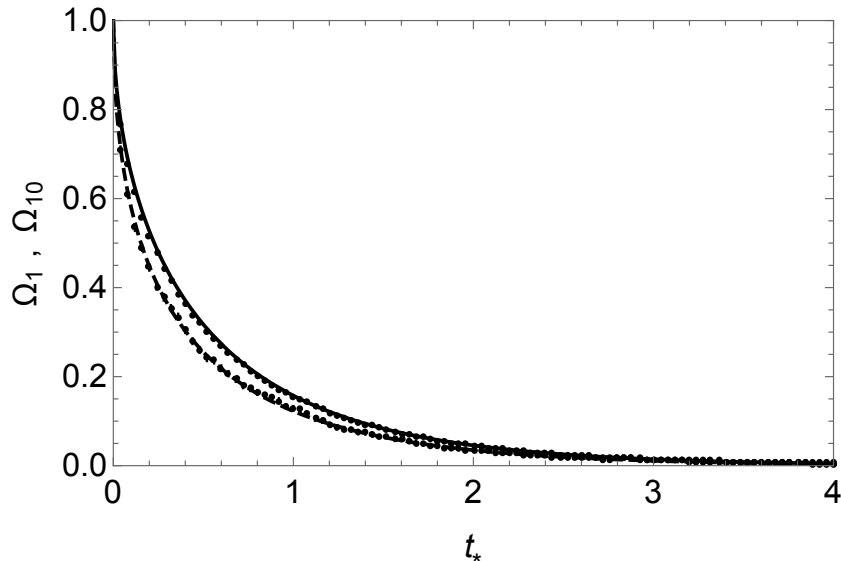


FIG. 3. Overlap ratios for $n = 1, 10$ (dots) plotted against a scaled time t_* , see (43), calculated in the discrete-time formalism, compared to theoretical results calculated in the continuous-time formalism using equations (45) (dashed line) and (57) (solid line), respectively. Discrete-time data points are calculated using Monte Carlo simulations for $\alpha = 1$, $N = 5000$, $\Delta t = 0.05$, repeated 5000 times to estimate the average overlap coefficient. Error bars are smaller than the size of the dots.

limit, where we can define the continuous physical time $t = k\Delta t$, corresponds to the double limit in which $\Delta t \rightarrow 0$ while $t = k\Delta t$ is constant. In this limit, the Fokker-Planck equation (1) is restored. If we additionally choose time units so that $\sigma^2 = 1$, then the system will be described by (7) with $\alpha = -2\mu > 0$ that we used to study the evolution of order statistics in the stationary state, which has an exponential distribution, with a probability density $p_{\text{stat}}(x) = \alpha e^{-\alpha x}$. For finite Δt , the stationary state in the discrete time formalism (59) may slightly differ from the exponential distribution. The finite size effects are very small for Δt of order 0.01. This is illustrated in Fig. 2 where the cumulative distribution function computed numerically for $\Delta t = 0.05$ is compared with the cumulative density function for the exponential distribution. The agreement is so good that no difference between the numerical points and the cumulative distribution for the exponential distribution can be detected with the naked eye.

To compute the overlap ratio in the discrete-time formalism, we simulate the evolution of a system of N particles according to (59). First, we generate a stationary state and register n leaders in this state. We treat this state as the initial state. We then continue the simulation and check how many leaders from the initial top- n list are on the top- n list at time k , i.e., what the overlap between these lists is, expressed as the number of leaders present on both lists. We repeat this experiment multiple times to calculate the average overlap and then normalize it to n , thus obtaining the average overlap ratio $\langle \Omega(k) \rangle$ over time k .

The result of the Monte Carlo simulations is shown in Fig. 3 where we compare the overlap ratio for $n = 1$ and $n = 10$ with theoretical results for $n = 1$ (45) and $n = \infty$ (57) obtained within the continuous-time formalism. We see that the two-formalisms give consistent results. We show results for $\alpha = 1$ ($n = 1$ and $n = 10$), but we checked that also for other values of α and n they are consistent.

The finite- N corrections are also consistent in both formalisms, as shown in Fig. 4, where the average overlap ratio for $n = 1$ calculated analytically in (35) for the continuous-time formalism and numerically for the discrete-time formalism is plotted for two N . In general, the overlap ratio $\langle \Omega_n(t) \rangle$ should approach n/N for $t \rightarrow \infty$, which is equal to the probability of randomly selecting n participants from N . For the curves presented in the figure, the asymptotic values are $1/10$ and $1/20$, for $N = 10$ and 20 , respectively.

VI. UNIVERSALITY

To highlight the universality of the results, we have numerically studied the overlap ratios of four one-dimensional point processes, which find applications in various research areas.

The problem when it comes to fitting is how to identify the parameter α . For moderately large n , for example $n = 10$, we know that (58) is a good approximation. When integrating this quantity in time t over an interval $[0, T]$, one finds for

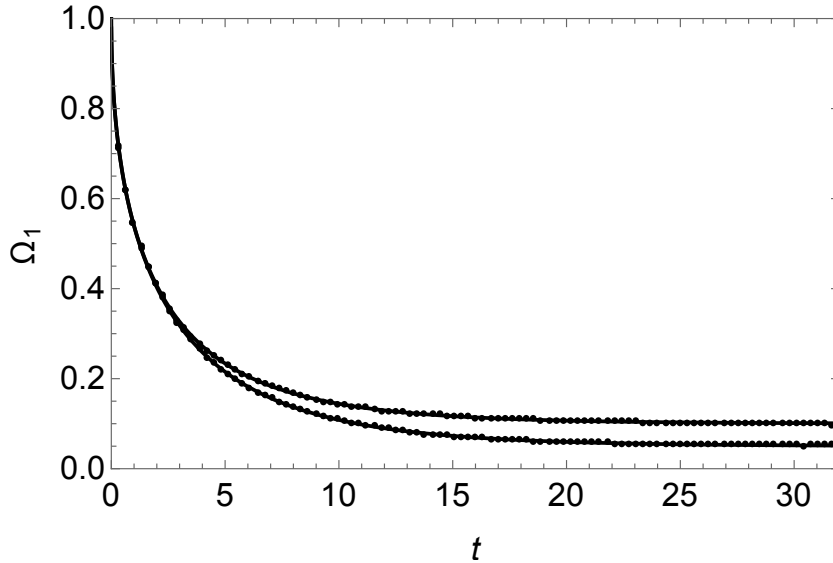


FIG. 4. Comparison of the overlap ratios for $n = 1$ for continuous time formalism (solid curves) calculated from Eq. (35) and for discrete time formalism calculated using Monte-Carlo simulations (dots). We upper and lower curves are for $N = 10, 20$, respectively. For large time t , the curves asymptotically approach the limiting value $1/N$, which is equal 0.1 and 0.05 for $N = 10, 20$, respectively. Each data point was calculated as an average from a sample of 5×10^5 of independent Monte-Carlo simulations. The size of the error bars is smaller than the size of the dots.

large $T \gg 1$ that

$$\int_0^T dt \langle \Omega(t) \rangle = \int_0^T dt \operatorname{erfc} \left(\sqrt{\frac{\alpha^2 t}{8}} \right) \sim \frac{4}{\alpha^2}. \quad (60)$$

The statistical error of this quantity is very low when it comes to numerical analysis because it is a integral.

A. Example 1: Brownian motion with position-dependent drift

The diffusion process on the half-axis that we have discussed so far is a representative of a broader class of diffusion models in one dimension with negative drift and a barrier limiting the range of diffusion from below. The equation describing processes of this class is a generalization of (59) and have the form

$$x_j(k) = x_j(k-1) + \hat{g}_j(k, x_j(k)). \quad (61)$$

The random factors \hat{g}_j are independent normal variables with variance Δt and mean $\mu(x)\Delta t$, especially the latter depends on the particle's position x as follows

$$\lim_{x \rightarrow \infty} \mu(x) = -\alpha/2 < 0 \quad (62)$$

and

$$\lim_{x \rightarrow -\infty} \mu(x) = +\infty. \quad (63)$$

The first condition means that there is an asymptotically constant negative drift for large x . The second condition implies that there is a barrier that limits the range of diffusion from below.

The corresponding equation in the continuous-time formalism (in Itô calculus) is

$$dx_j(t) = \mu(x_j)dt + dB_j(t) \quad (64)$$

where $B_j(t)$, $j = 1, \dots, N$ are independent Wiener processes. The corresponding Fokker-Planck equation

$$\partial_t p(x, t) = -\partial_x (\mu(x)p(x, t)) + \frac{1}{2} \partial_x^2 p(x, t) \quad (65)$$

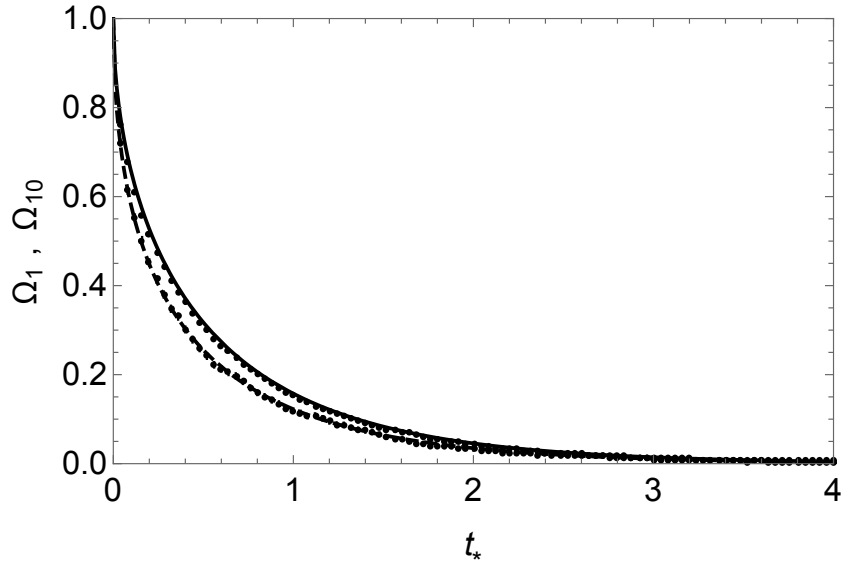


FIG. 5. Overlap ratio for $N = 5000$, $\alpha = 1$ and $\mu(x)$ given (67) for $n = 1$ and $n = 10$ obtained by averaging over 5000 Monte-Carlo samples (dots), compared to the theoretical Eqs. (45) (dashed line) and (57) (solid line).

has also a stationary state solution

$$p_{\text{stat}}(x) = \frac{1}{c_0} \exp \left[\int_0^x 2\mu(x') dx' \right] \quad \text{with} \quad c_0 = \int_{-\infty}^{\infty} dx \exp \left[\int_0^x 2\mu(x') dx' \right]. \quad (66)$$

For large positive x , the probability density behaves asymptotically as $p_{\text{stat}}(x) \sim e^{-\alpha x}$, which follows from (62). The second condition (63) dictates that $p_{\text{stat}}(x)$ is bounded from above by another exponential $\tilde{\gamma} e^{-\tilde{\alpha}|x|}$ with some positive constants $\tilde{\alpha}, \tilde{\gamma} > 0$ for large negative x . In fact, the behaviour at $x \rightarrow -\infty$ will drop faster than any exponential.

In Fig. 5 we show as an example the result of Monte Carlo calculations of the overlap ratio for $n = 1$ and $n = 10$ for the model with a soft barrier

$$\mu(x) = \begin{cases} -\alpha/2, & \text{for } x \geq 0, \\ -\alpha/2 + x^2/2, & \text{for } x < 0 \end{cases} \quad (67)$$

with $\alpha > 0$. As we can see in the figure, the overlap ratio is described by the same curve as for diffusion on \mathbb{R}_+ . More generally, for any model with constant negative drift $-\alpha/2 < 0$ for large x and a barrier from below, we expect the behavior of leaders to be shaped by an exponential tail $p_{\text{stat}}(x) \sim e^{-\alpha x}$ and thus described by the same universal formulas for the overlap ratios found in (50) and (57).

B. Example 2: overlap ratio for multiplicative stationary processes

If we interpret the stochastic process $x(t)$ as a logarithm of a random variable $w(t)$, that is, $x(t) = \ln w(t)$, then $\Delta x(t) = x(t + \Delta t) - x(t)$ is just the growth rate of $w(t)$ for the period from t to $t + \Delta t$. The quantity $w(t)$ undergoes a stochastic multiplicative process in which the growth rate is independent of $w(t)$ itself, which is known as Gibrat's law or the rule of proportional growth [12].

Generally, when the total growth rate $x(t)$ for the period from 0 to t grows unlimited when time t increases, $x(t)$ obeys normal (non-stationary) statistics with mean and variance increasing with t , and thus $w(t)$ obeys log-normal statistics. However, when the growth of the growth rate is limited by the presence of constant negative drift (and a barrier from below), then the growth rate has a stationary state with an exponential tail, that is, $p_{\text{stat}}(x) dx \sim e^{-\alpha x} dx$ for large x . Thus, the quantity w has a stationary state with a Pareto tail in the probability density function,

$$\tilde{p}_{\text{stat}}(w) dw \sim w^{-1-\alpha} dw, \quad (68)$$

which follows from changing $w = e^x$ in $p_{\text{stat}}(x) dx$.

Since the map $x \rightarrow w = e^x$ is strictly monotonously increasing, the order statistics for w is identical to the one of x . Therefore, the results (50) and (57) still apply to a class of Pareto distributions generated as stationary states of multiplicative stochastic processes.

In the ensuing subsections, we provide some evidence that the universality extends also to a broader class of mixed additive-multiplicative stochastic processes where the leaders effectively undergo multiplicative changes with drift of the effective growth rate towards smaller values.

C. Example 3: overlap ratio for the Bouchaud-Mézard model

The Bouchaud-Mézard model [19] describes the distribution of wealth in a population of individuals. The dynamics of the system is shaped by two factors, the rule of proportionate growth, which describes the growth of wealth of each individual and the redistribution of the wealth between interacting individuals. In the mean-field version of the model, the evolution of wealth is given by the following equations

$$w_j(k) = (1 - b)\tilde{w}_j(k) + \frac{b}{N} \sum_{l=1}^N \tilde{w}_l(k), \quad j = 1, \dots, N \quad (69)$$

where

$$\tilde{w}_l(k) = w_l(k-1)e^{g_l(k)}, \quad l = 1, \dots, N \quad (70)$$

and $g_l(k)$ are independently and identically distributed normal random numbers with mean $\mu\Delta t$ and variance $\sigma^2\Delta t$. The parameter Δt is the physical time between subsequent discrete times, which means between $k-1$ and k . The elements $\tilde{w}_j(k) = w_j(k-1)e^{g_j(k)}$ on the right-hand side correspond to the multiplicative changes in wealth described by Gibrat's rule $w_j(k-1) \rightarrow w_j(k-1)e^{g_j(k)}$. The parameter b is a redistribution factor. In the mean-field version of the model, wealth is redistributed according to the principle of proportionality, which says that a share of each individual's wealth, proportional to wealth itself, goes to a common pool from which all receive equal shares. The wealthiest contribute the most to the pot and receive much less from it as a result of redistribution. This is a kind of balancing mechanism that causes a stationary state to appear in the distribution of wealth. The parameter $b = \beta\Delta t$ depends linearly on Δt such as the mean $\mu\Delta t$ and the variance $\sigma^2\Delta t$. The coefficient β is the rate of wealth redistribution.

Actually, one is usually less interested in the absolute wealth of individuals, but more in the relative one. Hence, we consider the distribution of wealth of individual j relative to the average wealth at time k ,

$$v_j(k) = \frac{w_j(k)}{\frac{1}{N} \sum_{l=1}^N w_l(k)}. \quad (71)$$

In the continuum limit and for $N \rightarrow \infty$, the evolution equations for the relative wealth take the form (in the Itô convention)

$$dv_j(t) = \beta(1 - v_j(t))dt + \sigma v_j(t)dB_j(t). \quad (72)$$

They are identical for all j and they are decoupled from each other for $N \rightarrow \infty$ as then $N^{-1} \sum_{l=1}^N w_l(k)$ converges to a random number which is asymptotically independent of $w_j(k)$. Therefore, one can write a Fokker-Planck equation (independent of j)

$$\partial_t p(v, t) = \beta \partial_v ((v-1)p(v, t)) + \frac{\sigma^2}{2} \partial_v^2 (v^2 p(v, t)) \quad (73)$$

The equation has a stationary state solution given by the inverse Gamma distribution with the probability density

$$\tilde{p}_{\text{stat}}(v) = \frac{c}{v^{1+\alpha}} \exp\left[-\frac{\alpha-1}{v}\right], \quad (74)$$

where $\alpha = 1 + 2\beta/\sigma^2 > 0$ and $c = (\alpha-1)^\alpha/\Gamma(\alpha)$. By construction, the mean of the distribution is one, $\int v p_v(v) dv = 1$, reflecting the normalization (71).

We note that the power $\alpha = 1 + 2\beta/\sigma^2$ is independent of the drift μ . This is because μ is identical for all j and, therefore, cancels out in the definition of relative wealth (71). In this model, the role of negative drift comes from wealth redistribution, controlled by β . Redistribution has the greatest impact on reducing the relative wealth of the richest. The dependence on μ remains in the expression for average wealth, which for $N \rightarrow \infty$ behaves on average like

$$\left\langle \frac{1}{N} \sum_{l=1}^N w_l(t) \right\rangle = w_0 \exp\left[\left(\mu + \frac{\sigma^2}{2}\right)t\right]. \quad (75)$$

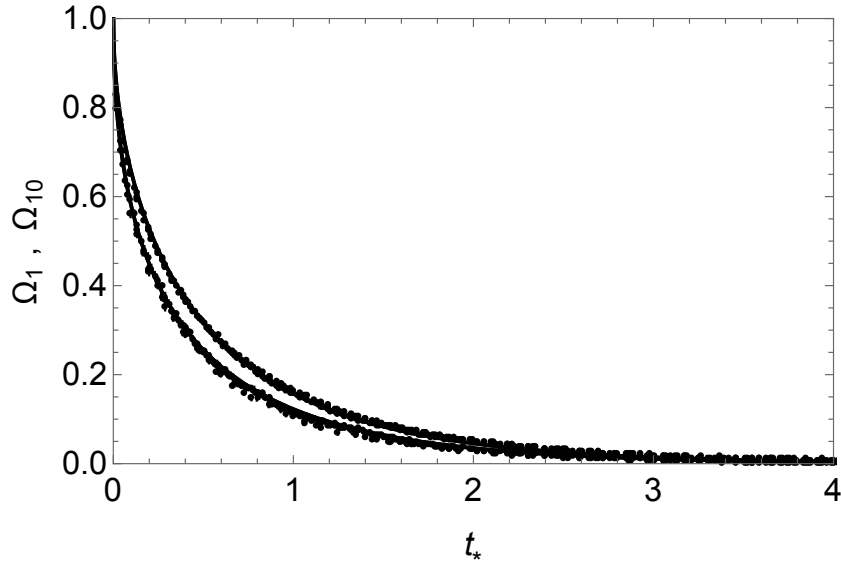


FIG. 6. Overlap ratios for $N = 3000$, $n = 1, 10$ and $\alpha = 2, 3, 4, 5$ for the Bouchaud-Mézard model computed using 5000 Monte Carlo samples. The data points are plotted against rescaled time $t_* = s(\alpha)t$, with $s = 0.48, 1.03, 1.66, 2.4$ for $\alpha = 2, 3, 4, 5$, respectively. This choice of the scaling factor $s(\alpha)$ makes the points for different α collapse to the curves given by Eqs. (45) and (57). These curves are depicted as continuous lines that are almost invisible in the crowd of data points.

For large v the distribution has a Pareto tail. Considering the discussion in subsection VI B, we would, therefore, expect that our prediction should hold true in this case. In Fig. 6, we show the comparison of the overlap ratio for $n = 1$ and $n = 10$ obtained in Monte Carlo simulation of the Bouchaud-Mézard model for different values of α and the analytical results (45) and (57) for the diffusion on \mathbb{R}_+ . To collapse the data, we rescaled the time variable $t_* = s(\alpha)t$. The scaling factors in Fig. 6 are $s = 0.48, 1.03, 1.66, 2.4$ for $\alpha = 2, 3, 4, 5$, respectively. The scaling factors are different from $s = \alpha^2/8 = 0.5, 1.125, 2, 3.125$, which would result from Eq. (43) for $\alpha = 2, 3, 4, 5$. This difference can be attributed to finite-size effects. To see this, let us rewrite Eq. (72) in the variable $x = \ln v$. Using Itô's lemma, we get

$$dx_j(t) = -(\beta + \sigma^2/2 - \beta e^{-x_j(t)})dt + \sigma dB_j(t) \quad (76)$$

or equivalently

$$dx_j(\tilde{t}) = -\frac{1}{2} \left(\alpha - (\alpha - 1)e^{-x_j(\tilde{t})} \right) d\tilde{t} + dB_j(\tilde{t}) \quad (77)$$

where $\alpha = 1 + 2\beta/\sigma^2$ and $\tilde{t} = \sigma^2 t$. We see that this equation is of the form (64) which describes Brownian motion in the presence of drift, discussed in section VI A. In the present case, the drift is related to α as

$$-2\mu(x) = \alpha - (\alpha - 1)e^{-x} \equiv \alpha_{\text{eff}}(x). \quad (78)$$

The value of drift approaches $-\alpha/2$ for $x \rightarrow \infty$, for finite x however it is equal to $-\alpha_{\text{eff}}(x)/2$. For systems of finite size, the drift should be calculated for the position of leaders, which are located at finite x . The position of the leader, x_1 , in a population of N elements, can be estimated as quantile of the stationary distribution for $1 - 1/N$ which gives

$$\frac{\gamma(\alpha, (\alpha - 1)e^{-x_1})}{\Gamma(\alpha)} = 1/N. \quad (79)$$

where $\gamma(\alpha, y) = \int_0^y t^{\alpha-1} e^{-t} dt$ is the lower incomplete Gamma function. The expression on the left-hand side is the value of the complementary cumulative distribution function for $v_1 = e^{x_1}$ of the inverse gamma distribution (74), which is the stationary state. From this equation one can estimate that

$$e^{-x_1} \approx \frac{(\Gamma(\alpha + 1)/N)^{1/\alpha}}{\alpha - 1} \quad (80)$$

which, after inserting to Eq. (78), gives

$$\alpha_{\text{eff}}(x_1) \approx \alpha - (\Gamma(\alpha + 1)/N)^{1/\alpha}. \quad (81)$$

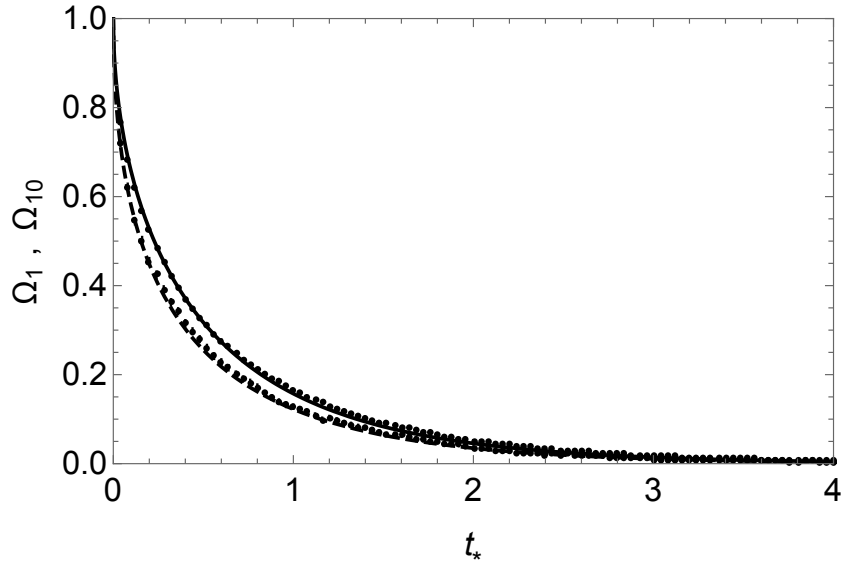


FIG. 7. Overlap ratios $\langle \Omega_n(t) \rangle$ for $n = 1, 10$ for the gas of $N = 5000$ particles whose positions are generated by independently identically distributed Kesten processes $w(t) = a(t)w(t-1) + b(t)$ with a, b being independently identically distributed log-normal processes $a \sim \ln N(\mu_a, \sigma_a^2)$ with $\mu_a = -0.1$, $\sigma_a^2 = 0.1$, and $b \sim \ln N(\mu_b, \sigma_b^2)$ with $\mu_b = -5$, $\sigma_b^2 = 0.01$. The asymptotic properties of the stationary distribution has a Pareto tail with the exponent $\alpha = -2\mu_a/\sigma_a^2 = 2$. The overlap is plotted against the universal variable $t_* = \alpha^2 t/8$, where $t = k\sigma_a^2$. The data points are compared to the analytic curves $\Omega_1(t_*)$ in (45) and $\Omega_*(t_*)$ in (57) derived for the diffusion on \mathbb{R}_+ .

Setting $N = 3000$ as in Fig. 6, we obtain from (80)

$$s_{\text{eff}} = \frac{\alpha_{\text{eff}}^2(x_1)}{8} \approx 0.487, 1.032, 1.712, 2.503 \quad (82)$$

and from a numerical solution of (79)

$$s_{\text{eff}} = \frac{\alpha_{\text{eff}}^2(x_1)}{8} \approx 0.487, 1.030, 1.694, 2.444 \quad (83)$$

for $\alpha = 2, 3, 4, 5$, respectively. These numbers are extremely close to those used as scaling factors in Fig. 6, which means that finite-size corrections explain the deviation of the scaling factor from its asymptotic value. The remaining deviations (which is less than 2%) can come from statistical errors and the other approximations done in our argumentation. For instance, the numerical fit is actually an average of the $n = 1$ and $n = 10$ fit which should have slightly different effective α_{eff} due to the variation of the positions of the individual largest particles.

To conclude this example, it is worth noting that in this model $x_j(t) - x_j(0)$ is the cumulative growth rate above the average inflation level for the entire system (see Eq. (71)).

D. Example 4: Overlap ratio for positive stationary Kesten processes

Another example where the same universality of the rank statistics of the leading particles can be expected is a system of N particles whose positions evolve according to Kesten processes [20]

$$w_j(k) = a_j(k)w_j(k-1) + b_j(k). \quad (84)$$

The random variables a_j and b_j are identical independent processes consisting of independently identically distributed positive random numbers. If initially the particles lie in the positive half-axis, then they will stay there during the whole process.

The system has a stationary state if the expectation values $\langle \ln a \rangle < 0$ and $\langle b \rangle < \infty$ are satisfied. We skipped the index j , here, because the processes are identical. The stationary state has a distribution with a Pareto tail $\tilde{p}_{\text{stat}}(w)dw \sim w^{-1-\alpha}dw$ if $\langle a^\alpha \rangle = 1$, $\langle a^{\alpha+1} \rangle < \infty$ and $\langle b^\alpha \rangle < \infty$. Actually, there are some additional conditions to exclude interferences between a and b , see [20, 21] for details.

As an example, consider $a_j(k)$ and $b_j(k)$ identical independent lognormal processes $a_j \sim \ln \mathcal{N}(\mu_a, \sigma_a^2)$ and $b_j \sim \ln \mathcal{N}(\mu_b, \sigma_b^2)$, with $\mu_a < 0$. In this case, the associated Kesten process has a stationary distribution with a Pareto tail with index $\alpha = -2\mu_a/\sigma_a^2$. Physical time t can be calculated from the discrete time k using the formula $t = k\Delta t = k\sigma_a^2$.

The result of the numerical simulation is shown in Fig. 7. The overlap ratios are very well described by the analytic formulas (45) and (57) that has been used for diffusion on \mathbb{R}_+ . The result can be intuitively understood as follows. Iterating (84) leads to

$$w(k) = a(k) \dots a(1)w(0) + \sum_{s=1}^k a(k) \dots a(s+1)b(s) \quad (85)$$

The associated process $x(k) = \ln w(k)$ is for large x mainly shaped by the leading product of the random variables $a(j)$ which after taking the logarithm makes $x(k)$ to behave for large x as an almost additive process with negative drift. For smaller x , on the other hand, a soft barrier is created by adding a positive value b in each step of the process, which makes values of $x(k)$ bounce towards larger values. In many respects, the situation is similar to diffusion, discussed in Sect. VI, which has a constant negative drift asymptotically for $x \rightarrow +\infty$ and a soft reflective barrier at some finite x .

VII. CONCLUSIONS

We have studied the overlap ratio that captures the fluctuations of the top n ranking of the particles. Especially, we derived a benchmark in the limit of a large number of particles when the statistics of the largest ranked particles is governed by independent and identical Brownian motions with a diffusion coefficient σ^2 and a drift $\mu < 0$. Remarkably, this benchmark for the top n depends only on the rescaled time $t_* = \mu^2 t / 2\sigma^4$ for finite n , see (50), as well as for $n \gg 1$, see (57). One consequence of these results is that without a drift the reshuffling of the ranking will be strongly suppressed. Stochastic fluctuations will never be strong enough to mix the top n with the remaining participants.

Furthermore, we have seen that even for moderate n of the top n , say about $n = 10$, the result for $n \gg 1$ is a very good approximation. This is particularly important as the result

$$\langle \Omega(t) \rangle \stackrel{n \gg 1}{\approx} \operatorname{erfc} \left(\sqrt{\frac{\mu^2 t}{2\sigma^4}} \right) \quad (86)$$

is extremely simple and does not require any elaborate numerical evaluation. When comparing this result with empirical data, it is very important to take the effective drift $\mu < 0$ and diffusion coefficient σ^2 of the top particles, which could be different from the average drift and diffusion of the bulk of the particles. To avoid an elaborate measurement of these quantities we suggest to measure the integrated time behaviour

$$\int_0^T dt \langle \Omega(t) \rangle \stackrel{T \gg 1}{\approx} \frac{\sigma^4}{\mu^2}. \quad (87)$$

for suitably large times T . This sets the proper time scale and has a small statistical error.

This effective drift and diffusion coefficient explains why the best agreement with the benchmark we derived can be found for a stationary state. Once the considered system is in a stationary state, the reshuffling of the ranking of various processes follows the benchmarks (50) and (57). We found perfect agreement with numerical simulations of a Brownian motion with a position-dependent drift and a lower soft barrier, the geometric Brownian motion, the Bouchaud–Mézard wealth distribution model [19], and Kesten processes [20]. What remains a challenge is to relate the system parameters of each of the respective processes to the effective ratio of the drift and diffusion coefficients for the top particles n . Such analytical relations are not always obvious, as could have been seen in the Bouchaud–Mézard model. In the extreme case that such a relation is elusive, one has to resort to measurement (87).

Finally, we would like to point out that the benchmarks we derived apply to Gumbel statistics for the extreme values, which in particular describes the statistics of top values in the stationary state of Brownian motion on a half-line. When going over to the other two universal extreme value statistics following the Fisher–Tippett–Gnedenko theorem [15, 24, 25] that is the Weibull law (in the case there is a hard wall in the vicinity of the top n that cannot be passed) and the Fréchet law (for cases where the stochastic process is heavy-tailed for the top n due to Lévy flights), we expect other behaviour. Actually, we think that the shuffling of the bottom n for the Brownian motion close to the reflective wall will follow Weibull statistics. We leave this issue for future research.

Another category of stochastic processes that shape complex systems in many situations is those based on growth rather than reshuffling. In many systems, growth is driven by preferential attachment [26–28] leading to heavy-tailed statistics. The values of local quantities describing the state of the system (for instance, degree of nodes in network models) generated in such growth processes are correlated with attachment time [29], and in this case the reshuffling

of extreme values is very limited, which is reflected in rank statistics [2, 30]. It would be interesting to calculate the overlap ratio for such growing processes, as was done here for random reshuffling. The overlap ratio could then serve as a benchmark that would help to distinguish the influence of stochastic reshuffling versus growth on the top-rank statistics.

ACKNOWLEDGMENTS

MK is partially funded by the Australian Research Council through the Discovery Project grant DP250102552, by the Alexander-von-Humboldt Foundation, and by the Swedish Research Council under grant no. 2021-06594 while the author was in residence at the Mittag-Leffler Institute in Djursholm, Sweden, during November/December of 2024. MK is also grateful to the Faculty of Physics and Applied Computer Science at the AGH University of Krakow and the Faculty of Physics of the University of Duisburg-Essen for their hospitality during his sabbatical.

Appendix A: Derivation of the heat kernel

In the first step to solve (7) and (8), we write the probability density $p(x, t)$ in terms of a mixed Fourier-Laplace transform

$$p(x, t) = \int d\omega dk \exp[-\omega t + ikx] \hat{p}(k, \omega). \quad (\text{A1})$$

When plugging this into the Fokker-Planck equation (7) we arrive at which leads to

$$0 = \int d\omega dk \left(\frac{1}{2}k^2 - \frac{i\alpha}{2}k - \omega \right) \hat{p}(k, \omega) = \int d\omega dk \frac{1}{2} (k - k_+(\omega)) (k - k_-(\omega)) \hat{p}(k, \omega) \quad (\text{A2})$$

where

$$k_{\pm}(\omega) = \frac{1}{2} \left(i\alpha \pm \sqrt{8\omega - \alpha^2} \right). \quad (\text{A3})$$

Therefore, the Fourier-Laplace transform $\hat{p}(k, \omega)$ must have the form

$$\hat{p}(k, \omega) = \delta(k - k_+(\omega)) \hat{p}_+(\omega) + \delta(k - k_-(\omega)) \hat{p}_-(\omega), \quad (\text{A4})$$

where $p_{\pm}(\omega)$ are yet some unknown functions of ω .

Performing the integral over k in (A1) yields

$$p(x, t) = \int_{\alpha^2/8}^{\infty} d\omega e^{-\omega t} \left(e^{ik_+(\omega)x} \hat{p}_+(\omega) + e^{ik_-(\omega)x} \hat{p}_-(\omega) \right). \quad (\text{A5})$$

The lower terminal of ω at $\alpha^2/8$ takes into account that the factors $e^{ik_{\pm}(\omega)x}$ have an oscillating (trigonometric) parts and a common exponential decay due to the constant drift, or equivalently that (A3) has a form

$$ik_{\pm}(\omega) = \frac{1}{2} (-\alpha \pm i\kappa). \quad (\text{A6})$$

where $\kappa = \sqrt{8\omega - \alpha^2}$ is a non-negative real number. After substituting $\omega = (\kappa^2 + \alpha^2)/8$, we arrive at

$$p(x, t) = \int_0^{\infty} d\kappa \exp\left(-\frac{(\kappa^2 + \alpha^2)t}{8}\right) \left[\exp\left(\frac{(-\alpha + i\kappa)x}{2}\right) \hat{q}_+(\kappa) + \exp\left(\frac{(-\alpha - i\kappa)x}{2}\right) \hat{q}_-(\kappa) \right]. \quad (\text{A7})$$

where $\hat{q}_{\pm}(\kappa)$ are derived from $p_{\pm}(\omega)$ by the change of variables.

Next, we try to satisfy the boundary condition (8), which become

$$0 = \alpha p(0, t) + \partial_x p(0, t) = \int_0^{\infty} d\kappa \exp\left(-\frac{(\kappa^2 + \alpha^2)t}{8}\right) \left[\frac{\alpha + i\kappa}{2} \hat{q}_+(\kappa) + \frac{\alpha - i\kappa}{2} \hat{q}_-(\kappa) \right]. \quad (\text{A8})$$

Therefore, the functions $\hat{q}_+(\kappa)$ and $\hat{q}_-(\kappa)$ must be related. Indeed, the expression in the square brackets must be identically equal to zero because the integral must vanish for all $t > 0$. We can express the two functions $\hat{q}_{\pm}(\kappa)$ in terms of a single odd but otherwise unknown function $\hat{q}(k)$,

$$\hat{q}_{\pm}(\kappa) = \frac{\mp\alpha + i\kappa}{2} \frac{\hat{q}(\kappa)}{2i} \quad (\text{A9})$$

Then, the probability density (A7) is equal to

$$p(x, t) = \int_0^\infty d\kappa \exp\left(-\frac{(\kappa^2 + \alpha^2)t}{8}\right) \left[\frac{-\alpha + i\kappa}{2} \exp\left(\frac{(-\alpha + i\kappa)x}{2}\right) + \frac{\alpha + i\kappa}{2} \exp\left(\frac{(-\alpha - i\kappa)x}{2}\right) \right] \frac{\hat{q}(\kappa)}{2i} \quad (\text{A10})$$

or equivalently

$$p(x, t) = \partial_x \int_0^\infty d\kappa \exp\left(-\frac{(\kappa^2 + \alpha^2)t}{8} - \frac{\alpha x}{2}\right) \sin\left(\frac{\kappa x}{2}\right) \hat{q}(\kappa). \quad (\text{A11})$$

Finally, we need to implement the initial condition in (8) that fixes the function $\hat{q}(k)$. Especially, they are related as follows

$$p_0(x) = p(x, 0) = \partial_x \int_0^\infty d\kappa \exp\left(-\frac{\alpha x}{2}\right) \sin\left(\frac{\kappa x}{2}\right) \hat{q}(\kappa). \quad (\text{A12})$$

The integration of both sides in x is equal to

$$\int_0^x p(\xi, 0) d\xi = \exp\left(-\frac{\alpha x}{2}\right) \int_0^\infty d\kappa \sin\left(\frac{\kappa x}{2}\right) \hat{q}(\kappa). \quad (\text{A13})$$

This expression involves the cumulative density function $P_-(x, 0)$ of the initial condition. In general we denote the probability that the particle at time t is in the interval $[0, x]$ by

$$P_-(x, t) = \int_0^x d\xi p(\xi, t), \quad (\text{A14})$$

When introducing

$$q(x) \equiv \exp\left(\frac{\alpha x}{2}\right) \int_0^x d\xi p(\xi, 0) = \exp\left(\frac{\alpha x}{2}\right) P_-(x, 0) \quad (\text{A15})$$

where and inserting it into (A13), it becomes imminent that $q(x)$ is just the Fourier sine-transform of $\hat{q}(\kappa)$, i.e.

$$q(x) = \int_0^\infty d\kappa \sin\left(\frac{\kappa x}{2}\right) \hat{q}(\kappa). \quad (\text{A16})$$

The inverse transform is given by

$$\hat{q}(\kappa) = \frac{1}{\pi} \int_0^\infty dx \sin\left(\frac{\kappa x}{2}\right) q(x) = \frac{1}{\pi} \int_0^\infty dx \sin\left(\frac{\kappa x}{2}\right) \exp\left(\frac{\alpha x}{2}\right) P_-(x, 0) \quad (\text{A17})$$

which, once inserted into an integrated form of (A11), leads to the solution

$$\begin{aligned} P_-(x, t) &= \int_0^\infty d\kappa \exp\left(-\frac{(\kappa^2 + \alpha^2)t}{8} - \frac{\alpha x}{2}\right) \sin\left(\frac{\kappa x}{2}\right) \frac{1}{\pi} \int_0^\infty dy \sin\left(\frac{\kappa y}{2}\right) \exp\left(\frac{\alpha y}{2}\right) P_-(y, 0) \\ &= \exp\left(-\frac{\alpha^2 t}{8}\right) \int_0^\infty dy \exp\left(\frac{\alpha(y-x)}{2}\right) P_-(y, 0) \frac{1}{\pi} \int_0^\infty d\kappa \exp\left(-\frac{\kappa^2 t}{8}\right) \sin\left(\frac{\kappa x}{2}\right) \sin\left(\frac{\kappa y}{2}\right). \end{aligned} \quad (\text{A18})$$

In the second line, we interchanged the order of integration. The latter allows us to integrate over κ , which is equal to a sum of two non-centred Gaussian integrals,

$$\frac{1}{\pi} \int_0^\infty d\kappa \exp\left(-\frac{\kappa^2 t}{8}\right) \sin\left(\frac{\kappa x}{2}\right) \sin\left(\frac{\kappa y}{2}\right) = \frac{1}{\sqrt{2\pi t}} \left[\exp\left(-\frac{(x-y)^2}{2t}\right) - \exp\left(-\frac{(x+y)^2}{2t}\right) \right]. \quad (\text{A19})$$

Putting this into the above equation we get the equation for the evolution of the cumulative density function

$$P_-(x, t) = \int_0^\infty dy P_-(y, 0) L(y, x, t) \quad (\text{A20})$$

with the propagation kernel

$$L(y, x, t) = \frac{1}{\sqrt{2\pi t}} \exp\left(-\frac{\alpha^2 t}{8}\right) \exp\left(\frac{\alpha(y-x)}{2}\right) \left[\exp\left(-\frac{(x-y)^2}{2t}\right) - \exp\left(-\frac{(x+y)^2}{2t}\right) \right]. \quad (\text{A21})$$

The kernel $L(y, x, t)$ is related to the function $F(y, x, t)$ in (11) as follows

$$L(y, x, t) = -\partial_y F(y, x, t) = \frac{1}{\sqrt{2\pi t}} \exp\left(-\frac{(2(y-x) - \alpha t)^2}{8t}\right) - \frac{e^{-\alpha x}}{\sqrt{2\pi t}} \exp\left(-\frac{(2(y+x) - \alpha t)^2}{8t}\right). \quad (\text{A22})$$

We plug this relation into (A20) and integrate by parts to find

$$P_-(x, t) = \int_0^\infty dy p(y, 0) F(y, x, t). \quad (\text{A23})$$

The boundary terms are vanishing as either $P_-(y=0, 0) = 0$ or $F(y=\infty, x, t) = 0$. Taking the derivative of both sides with respect to x and using (12), we finally arrive at the claim (9).

Appendix B: Sum rules

We first check the sum rules (19) in the sum over j as it is simpler compared to (28). When exploiting the expression in terms of the contour integral in z in (18), we can understand the sum combined with the derivative in x as the explicit form of the product rule. For the second expression in (18), this is

$$\sum_{j=1}^N P(k; j; t | y_1, \dots, y_N) = \oint \frac{dz}{2\pi i z^k (1-z)} \int_0^\infty dx \partial_x \left(\prod_{l=1}^N (z + (1-z)F(y_l, x, t)) \right) = \oint \frac{dz(1-z^N)}{2\pi i z^k (1-z)} = 1. \quad (\text{B1})$$

In the second equality, we used $F(y, 0, t) = 0$ and $F(y, \infty, t) = 1$, and in the last one we exploited the geometric sum in combination with $k \leq N$.

The second identity in (19) is also straightforward. The sum over k is a geometric sum which gives

$$\sum_{k=1}^N P(k; j; t | y_1, \dots, y_N) = \int_0^\infty dx \oint \frac{dz}{2\pi i z^N} \frac{1-z^N}{1-z} \partial_x F(y_j, x, t) \prod_{l \neq j} (z + (1-z)F(y_l, x, t)). \quad (\text{B2})$$

The integrand is a meromorphic function in z with the only poles in $z = 0$ and $z = \infty$. When choosing the contour as a circle with $|z| > 1$, then we notice that the integral over the first term proportional to $1/(1-z)$ must vanish as it is holomorphic at $z = \infty$ and the only poles lie inside the contour, meaning we can shift the contour to infinity where the integrand vanishes.

For the second term proportional to $z^N/(1-z)$ the pole at the origin is removed and the newly created pole at $z = 1$ is simple for which the residue theorem yields

$$\sum_{k=1}^N P(k; j; t | y_1, \dots, y_N) = \int_0^\infty dx \oint \frac{dz}{2\pi i z^N} \frac{1-z^N}{1-z} \partial_x F(y_j, x, t) \prod_{l \neq j} (1 + 0 \cdot F(y_l, x, t)) = \int_0^\infty dx \partial_x F(y_j, x, t) = 1 \quad (\text{B3})$$

The last equality is clear due to $F(y, 0, t) = 0$ and $F(y, \infty, t) = 1$.

Now, we move on to prove (28). We first apply the geometric sum

$$\sum_{k=1}^N P(k; j; t | p_0) = N \int_0^\infty dx \int_0^\infty dr K(r, x, t) p_0(r) \oint \frac{dz}{2\pi i z^j} \oint \frac{dw}{2\pi i w^N} \frac{1-w^N}{1-w} (w P_z(r) + (1-w) G_z(r, x, t))^{N-1}. \quad (\text{B4})$$

We recall the definitions (24) and (25). Like before, the integrand is meromorphic in w with the only poles at the origin and infinity allowing us to choose the contour along $|w| = 2$, for example. However, when the integrand is divided into one term proportional to $1/(1-w)$ and another term proportional to $w^N/(1-w)$, the first term must vanish, as all singularities of this term lie inside the contour, while the second term can be evaluated at the only residue at $w = 1$. Thence, it is

$$\begin{aligned} \sum_{k=1}^N P(k; j; t | p_0) &= N \int_0^\infty dx \int_0^\infty dr K(r, x, t) p_0(r) \oint \frac{dz}{2\pi i z^j} P_z^{N-1}(r) \\ &= N \int_0^\infty dx \int_0^\infty dr K(r, x, t) p_0(r) \binom{N-1}{j-1} P_0^{N-j}(r) (1 - P_0(r))^{j-1}. \end{aligned} \quad (\text{B5})$$

In the second line we have carried the second contour integral over z . Finally, we substitute $R = P_0(r) \in [0, 1]$ and find the desired result

$$\sum_{k=1}^N P(k; j; t|p_0) = N \int_0^\infty dx K(r, x, t) \binom{N-1}{j-1} \overbrace{\int_0^1 dR R^{N-j} (1-R)^{j-1}}^{=(N-j)!(j-1)!/N!} = \int_0^\infty dx K(r, x, t) = 1. \quad (\text{B6})$$

Finally, we consider the sum over j in (28) which can be calculated in a similar way. Firstly, we rewrite the function in the parentheses of (26) as follows

$$wP_z(r) + (1-w)G_z(r, x, t) = z[w + (1-w)G(x, t)] + (1-z)[wP_-(r) + (1-w)G_-(r, x, t)] \quad (\text{B7})$$

where

$$G(x, t) = G_-(r, x, t) + G_+(r, x, t) = \int_0^\infty F(r', x, t)p_0(r')dr'. \quad (\text{B8})$$

We note that $G(0, t) = 0$ and $G(\infty, t) = 1$ and also that

$$dG(x, t) = dx \int_0^\infty K(r, x, t)p_0(r)dr. \quad (\text{B9})$$

Using this observation, we evaluate the sum along the very same lines as in Eqs. (B4-B6) and find

$$\begin{aligned} \sum_{j=1}^N P(k; j; t|p_0) &= N \int_0^\infty dx \int_0^\infty dr K(r, x, t)p_0(r) \\ &\times \oint \frac{dw}{2\pi iw^k} \oint \frac{dz}{2\pi iz^N} \frac{1-z^N}{1-z} (z[w + (1-w)G(x, t)] + (1-z)[wP_-(r) + (1-w)G_-(r, x, t)])^{N-1} \quad (\text{B10}) \\ &= N \int_0^\infty dx \int_0^\infty dr K(r, x, t)p_0(r) \oint \frac{dw}{2\pi iw^k} (w + (1-w)G(x, t))^{N-1} = 1, \end{aligned}$$

which has been to be shown.

Appendix C: Asymptotic behavior of the integral (53)

Let us rewrite (53) as

$$\Omega_{*n}(t_*) = \frac{e^{-t_*}}{n\sqrt{\pi}} \int_{-\infty}^\infty ds e^{-s^2} \oint \frac{dz}{2\pi iz} \frac{q}{(1+z^{-1})(1+z)} (1 - (1+z^{-1})\sigma_-)^n [(1 - (1+z)\sigma_+)^n - 1] \quad (\text{C1})$$

where $q = q(s, t_*)$ (47) and

$$\sigma_\pm = \sigma_\pm(s, t_*) = \frac{e^{\pm 2s\sqrt{t_*}}}{q(s, t_*)}. \quad (\text{C2})$$

In the following discussion we will take advantage of the inequality

$$0 < \sigma_\pm < 1. \quad (\text{C3})$$

The inequality on the left side is obvious, while the one on the right side can be proven using the integral representation of $q(s, t_*)$ (47)

$$q(s, t_*) = e^{\pm 2\sqrt{t_*}s} + \frac{2}{\sqrt{\pi}} \int_0^\infty e^{-(\lambda \pm s)^2 - t_*} \sinh(2\sqrt{t_*}\lambda) d\lambda > e^{\pm 2\sqrt{t_*}s}. \quad (\text{C4})$$

Dividing both sides by $q(s, t_*)$, we get $\sigma_\pm < 1$.

The original contour of integration over z in (C1) is a circle centered at zero of the radius $\epsilon \ll 1$. The radius can be increased without affecting the integral, provided that no new singularities appear inside the increased contour. The radius can be increased almost to unity, but not to unity, because then the contour would pass through the double pole

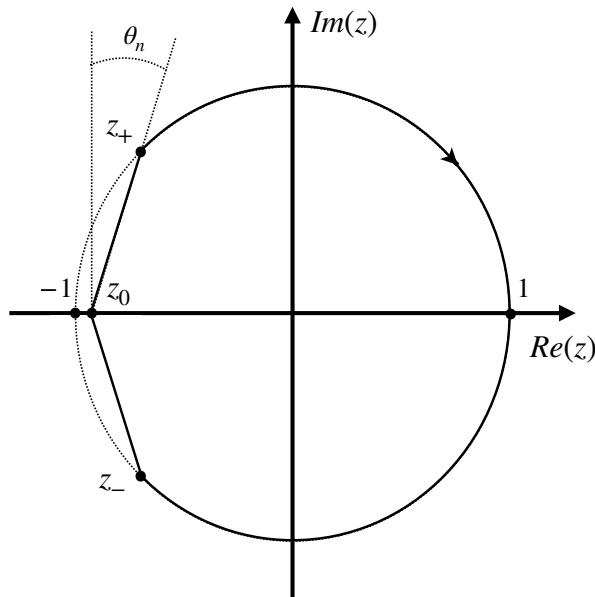


FIG. 8. The integration contour consists of two linear segments $[z_-, z_0]$, $[z_0, z_+]$ and the unit circle arc going clockwise from z_+ to z_- . The angle θ_n is between the vertical line (parallel to the imaginary axis) and the linear segment $[z_0, z_+]$. For $n \rightarrow \infty$, $\theta_n \rightarrow 0$.

at $z = -1$. The idea is to deform the contour into a shape that almost everywhere overlaps the unit circle, except the vicinity of the double pole, where it passes through the point at $z_0 = -1 + 1/n$, which is slightly away from the pole.

An example is the contour shown in Fig. 8.

$$z_{\pm} = - \left(1 - \frac{1}{n^{2/3}} \right) \pm i \sqrt{1 - \left(1 - \frac{1}{n^{2/3}} \right)^2} \quad (\text{C5})$$

and two line segments connecting the two points with the point $z_0 = -1 + 1/n$. In this way, we avoid the singularity at $z = -1$. For $n \rightarrow \infty$ the integral over the arc of the unit circle tends to zero, as the leading contributions of it will be found at z_{\pm} where the modulus of the integrand is of order $\mathcal{O}(n^{4/3} \exp[-n^{1/3}\sigma_-])$.

This means that the integrand exponentially tends to zero for all points on the arc of the unit circle in the limit $n \rightarrow \infty$. We needed to choose the bound with $1/n^{2/3}$ instead of the more natural $1/n$ scaling so that the whole unit circle is suppressed. For the naive choice, this would not have been the case.

What remains is the integral over the two line segments from z_+ to z_0 and the from z_0 to z_- . This integral is parametrised as follows

$$z = -1 + \frac{1 + ie^{-i \text{sign}(y)\theta_n} y}{n} \quad \text{with } y \in [-n|z_+ - z_0|, n|z_+ - z_0|] \quad (\text{C6})$$

where θ_n is the angle of the line segments to the imaginary axis. This angle is of the order $\mathcal{O}(n^{-1/3})$ and thus vanishes in the limit $n \rightarrow \infty$. The bounds of y behave like $n^{2/3}$ and hence tend to infinity so that we effectively integrate at the end over the whole line $z = -1 + (1 + iy)/n$, with $y \in (-\infty, +\infty)$. The powers $(\dots)^n$ in (C1) approach exponential functions for $n \rightarrow \infty$, so we arrive at (54).

-
- [1] M. Alvo and P. L. H. Yu, *Statistical Methods for Ranking Data*, Springer, Heidelberg, 2014.
[2] N. Blumm, G. Ghoshal, Z. Forró, M. Schich, G. Bianconi, J.-P. Bouchaud, and A.-L. Barabási, *Phys. Rev. Lett* **109**, 128701 (2012).
[3] Z. Burda, M. J. Krawczyk, K. Malarz, and M. Snarska, *Entropy* **23**, 842 (2021) [arXiv:2105.08048].
[4] G. Iñiguez, C. Pineda, C. Gershenson, and A.-L. Barabási, *Nature Communications* **13**, 1646 (2022) [arXiv:2104.13439].
[5] M. Wołoszyn and K. Kułakowski, *Physica A* **610**, 128402 (2023) [arXiv:2210.10484].
[6] F. De Domenico, F. Caccioli, G. Livan, G. Montagna, and O. Nicosini, [arXiv:2401.15968] (2024).

- [7] P. Dong, R. Han, B. Jiang, and Y. Xu, [arXiv:2406.16507] (2024).
- [8] D. S. Dean, Pi. Le Doussal, S. N. Majumdar, and G. Schehr, *J. Stat. Mech.* **2017**, 063301 (2017) [arXiv:1612.03954].
- [9] M. R. Evans and S. N. Majumdar, *J. Stat. Mech.* **2008**, P05004 (2008) [arXiv:0804.0197].
- [10] H. Guclu, G. Korniss, and Z. Toroczkai, *Chaos* **17**, 026104 (2007) [arXiv:cond-mat/0701301].
- [11] E. J. Gumbel, *Statistics of Extremes*, Dover, New York, 1958.
- [12] R. Gibrat, *Les Inégalités économiques*, Paris, 1931.
- [13] M. Levy and S. Solomon, *International Journal of Modern Physics C* **7**, 595 (1996) [arXiv:adap-org/9607001].
- [14] M. Levy and S. Solomon, *Physica A: Statistical Mechanics and its Applications* **242**, 90 (1997).
- [15] S. N. Majumdar, A. Pal, and G. Schehr, *Physics Reports* **840**, 1–32 (2020).
- [16] C. Spearman, *The American Journal of Psychology* **15**, 72 (1904).
- [17] M. G. Kendall, *Biometrika* **30**, 81 (1938).
- [18] B. Kjos-Hanssen, *J. Log. Comput.* **32**, 1611 (2022) [arXiv:2111.02498].
- [19] J.-P. Bouchaud and M. Mézard, *Physica A* **282**, 536 (2000), [arXiv:cond-mat/0002374].
- [20] H. Kesten, *Acta Math.* **131**, 207 (1973).
- [21] D. Buraczewski, et al., *Stochastic models with power-law tails*, Springer, Heidelberg, 2016.
- [22] J. M. Harrison, *Brownian Motion and Stochastic Flow Systems*, Wiley, New York, 1985.
- [23] J. Abate and W. Whitt, *Advances in Applied Probability*, **19**, 560 (1987).
- [24] R. A. Fisher and L. H. C. Tippett, *Mathematical Proceedings of the Cambridge Philosophical Society*, **24**, 180 (1928).
- [25] B. V. Gnedenko, *Ann. Math.* **44**, 423 (1943).
- [26] G. U. Yule, *Phil. Trans. Roy. Soc. Lond. B* **213**, 21 (1925).
- [27] H. A. Simon, *Biometrika*, **42**, 425, (1955).
- [28] A.-L. Barabási and R. Albert, *Science* **286**, 509 (1999), [arXiv:cond-mat/9910332].
- [29] P. L. Krapivsky and S. Redner, *Phys. Rev. E* **63**, 066123 (2001), [arXiv:cond-mat/0011094].
- [30] G. Ghoshal and A.-L. Barabási, *Nature Communications* **2**, 394 (2011).